Journal of the Optical Society of America B
OPTICAL PHYSICS

Light switching in microparticles based on half-space invisible states

A. R. Bekirov,* A. F. Uspenskiy, V. A. Sitnyansky, B. S. Luk'yanchuk, and A. A. Fedyanin

Faculty of Physics, Lomonosov Moscow State University, Moscow 119991, Russia
**bekirovar@my.msu.ru*

Received 28 April 2026; revised 22 June 2026; accepted 22 June 2026; posted 22 June 2026; published 20 July 2026

The control of light scattering by a microparticle through the excitation of non-radiating states in a half-space via engineering the incident field is demonstrated. By tuning the external field parameters, an 85% efficiency of redistribution of scattered light between the two half-spaces is achieved with only a 1.3% relative change in its refractive index. Spherical semiconductor particles of varying radii illuminated in the visible range, with refractive index modulation achieved via charge carrier injection, are considered. Using $Al_{0.1}Ga_{0.9}As$ as a model material, we analyze the feasibility of achieving efficient directional control of light scattering. The results provide insight into all-optical manipulation of light using tunable semiconductor structures.

https://doi.org/10.1364/JOSAB.603925

1. INTRODUCTION

Microparticles supporting Mie-type resonances provide a flexible platform for a wide range of optical phenomena arising from the interplay of particle shape and size, refractive index, excitation geometry, and local environment [1]. Under these conditions, a broad spectrum of phenomena emerges, including bound states in the continuum [2,3], super-resolution imaging [4], directional emission control [5], Kerker scattering [6], whispering-gallery modes [7], local field enhancement [8], and photonic nanojets [9]. By arranging these microparticles into engineered arrays (metasurfaces), one can exploit their resonant responses to achieve precise control over the amplitude, phase, polarization, and directionality of light at the subwavelength scale [10,11]. Among this class of phenomena, a new concept of half-space invisible states has recently been proposed [12], which were states in microparticles that arise from the interference of Mie-type modes excited within the particle, leading to the suppression of radiation in one half-space.

As photonic technologies advance, the development of active nanophotonic structures becomes increasingly important. Active elements—whose optical properties can be tuned by external electric or magnetic fields, temperature modulation, nonlinear absorption, or phase transitions—enable reconfigurable and programmable photonic functions [13,14]. Among the available control mechanisms, all-optical tuning is particularly appealing because it relies solely on light-induced changes, eliminating the need for electronic contacts and enabling operation on femtosecond and picosecond timescales [15,16]. When driven by ultrashort laser pulses, this mechanism enables switching speeds that far surpass those achievable through electro-optic or thermo-optic means [17], making all-optical switching one of the most promising directions for future ultrafast photonic systems.

The search for new methods of all-optical switching is one of the key tasks of modern nanophotonics. This paper analyzes the mechanisms underlying optical switching based on the excitation of half-space invisible states. Typically, studies assume a planar wavefront for the incident light. However, in this work, we depart from this assumption to study complex electromagnetic field distributions.

Various materials are considered in the literature to control light scattering. Here, we focus on $Al_{0.1}Ga_{0.9}As$—direct-bandgap III–V semiconductors with high refractive indices, strong $\chi^{(3)}$ nonlinearities, efficient multiphoton absorption pathways, and ultrafast carrier relaxation dynamics arising from rapid radiative recombination and intervalley scattering [18]. The Al concentration of 10% was chosen to match the material's bandgap with the Ti:sapphire laser frequency. These characteristics make it an ideal candidate for implementing ultrafast all-optical switching in high-index resonant microstructures.

2. METHODS

A. Scattering of Electromagnetic Waves by a Particle: T-Matrix Formalism and Control of Radiation Patterns

The scattering of electromagnetic waves by a particle can be effectively described using the T-matrix formalism [19], which establishes a relationship between the incident field and the field

scattered by the particle. We focus on homogeneous particles with a constant refractive index at a specific wavelength of light.

Both the incident field ($\mathbf{E}^{\text{inc}}$) and the scattered field ($\mathbf{E}^{\text{sca}}$) can be expressed in terms of expansion coefficients (g_{lm}, f_{lm}) and (b_{lm}, a_{lm}), respectively. These coefficients are derived from the representation of the fields using basis functions, commonly chosen as the vector spherical harmonics $\mathbf{M}_{lm}$ and $\mathbf{N}_{lm}$ [20]:

$$\mathbf{E}^{\text{inc}} = \sum_{l=1}^{l_{\max}} \sum_{m=-l}^{l} f_{lm}\mathbf{N}_{lm}^{(1)} + g_{lm}\mathbf{M}_{lm}^{(1)}, \tag{1}$$

$$\mathbf{E}^{\text{sca}} = \sum_{l=1}^{l_{\max}} \sum_{m=-l}^{l} a_{lm}\mathbf{N}_{lm}^{(3)} + b_{lm}\mathbf{M}_{lm}^{(3)}, \tag{2}$$

where $l_{\max}$ is the maximal number of excited modes, as determined by the convergence condition of series (1) and (2). The functions $\mathbf{N}$ and $\mathbf{M}$ are given by

$$\mathbf{M}_{lm}^{(1,3)} = z_l(\rho)e^{im\varphi}(i\pi_{lm}\mathbf{e}_\theta - \tau_{lm}\mathbf{e}_\varphi),$$

$$\mathbf{N}_{lm}^{(1,3)} = \rho^{-1}z_l(\rho)l(l+1)P_l^m(\cos\theta)e^{im\varphi}\mathbf{e}_r + \rho^{-1}[\rho z_l(\rho)]'e^{im\varphi}(\tau_{lm}\mathbf{e}_\theta + i\pi_{lm}\mathbf{e}_\varphi),$$

where the superscript$^{(1)}$ indicates that $z = j_l$, and $^{(3)}$ $z = h_l$, j_l and h_l are the spherical Bessel function and the Hankel function of the first kind, respectively, $\rho = kr$, where k is the wavenumber in the medium, $\pi_{lm} = m P_l^m(\cos\theta)/\sin\theta$, $\tau_{lm} = d P_l^m(\cos\theta)/d\theta$ and P_l^m is the associated Legendre polynomials and (r, θ, φ) are the spherical coordinates with the origin at the center of the particle. The T-matrix connects the columns of the incident field coefficients $E^i = (g_{lm}, f_{lm})$ and the scattered field coefficients $E^s = (b_{lm}, a_{lm})$, where the indices l and m span all possible values. If the particle is axisymmetric relative to the z axis, the coefficients with different m indices can be calculated independently:

$$E_m^s = T_m E_m^i. \tag{3}$$

In this relation, the index m is fixed for the vector columns E_m^i, E_m^s, while the index l spans all possible values, i.e., $l = \max(|m|, 1), |m|+1, |m|+2, \ldots, l_{\max}$. If the distance from the particle is much greater than the wavelength, i.e., $r \gg \lambda$, the scattered field can be expressed as

$$\mathbf{E}^{\text{sca}} = \mathbf{F}(\theta, \varphi)\exp(ikr)/(ikr), \tag{4}$$

where $\mathbf{F}$ is the scattering amplitude. The scattering amplitude $\mathbf{F}$ is expressed in terms of the expansion coefficients introduced in Eq. (2) and is written using two auxiliary functions, S_1 and S_2:

$$\mathbf{F}(\theta, \varphi) = S_1\mathbf{e}_\theta + S_2\mathbf{e}_\varphi. \tag{5}$$

The functions S_1 and S_2 are defined as follows:

$$\begin{aligned} S_1 &= -\textstyle\sum_{l,m}\exp(im\varphi)(-i)^{l+1}[a_{lm}\tau_{lm} + b_{lm}\pi_{lm}], \\ S_2 &= -\textstyle\sum_{l,m}\exp(im\varphi)(-i)^{l}[a_{lm}\pi_{lm} + b_{lm}\tau_{lm}]. \end{aligned} \tag{6}$$

We aim to achieve a sharp change in the radiation pattern $\mathbf{F}$ by varying the refractive index. Our approach for controlling the radiation pattern involves exciting non-radiating in half-space states in the particle through incident radiation. A particle is considered to be in a non-radiating state if the scattering coefficient vector E_m^s is a linear combination of the columns of a certain matrix Q_m. In this case, the scattering amplitude satisfies the following relationship:

$$\mathbf{F}(\theta, \varphi) \equiv 0, \text{ at } \theta \le \pi/2. \text{ If } E_m^s = Q_m E_m^Q, \tag{7}$$

where E_m^Q is an arbitrary vector of coefficients describing the linear combination. The matrix of half-space non-radiating states, Q_m, was first computed in [21], and this concept was further developed in [12]. Each column of the matrix Q_m represents a decomposition of the type (2) corresponding to the mode $\mathbf{N}_{l_0m_0}^{(3)}$ or $\mathbf{M}_{l_0m_0}^{(3)}$, in which the harmonics that propagate in the direction $z > 0$ are omitted. In this case, the coefficients a_{lm}, b_{lm} contain only modes with the same azimuthal number $m = m_0$. The orbital modes l include the mode with $l = l_0$, as well as modes with opposite parity, which decay as $|l - l_0|$ increases.

If the column E_m^s contains $l_{\max}$ modes, then to ensure that Eq. (7) is satisfied with high accuracy, the maximum mode number $l_0 = l_{\max}^Q$ in the E_m^Q must be less than $l_{\max}$. In our work, we chose $l_{\max}^Q = l_{\max} - 8$. Therefore, if $l_{\max} = 10$, for $m = 1$, the dimensions of the matrix $T_{m=1}$ will be 10×10, the dimensions of E_m^s and E_m^i will be 10×1, and the dimensions of the matrix $Q_{m=1}$ will be 10×2, while the column E_m^Q will be 2×1.

If we consider E_m^s as a linear combination of the complex conjugate matrix $(Q_{-m})^*$ with the opposite azimuthal index m, then the condition in Eq. (7) will hold in the opposite half-space, i.e., for $\theta \ge \pi/2$. This means that the particle will be non-radiating in the opposite direction.

B. Effect of Carrier Concentration on the Dispersion of Refractive Index and Absorption in AlGaAs

The change in the complex refractive index that occurs due to the injection of free charge carriers into the volume of the semiconductor can be described within the quantum model by three processes [18]: absorption by free carriers, bandfilling shrinkage, and filling of bands (Burstein–Moss effect). Free carrier absorption, which involves intraband transitions within the conduction band, contributes to the refractive index change according to the Drude model as follows:

$$\Delta n_{\text{FCA}} = -\frac{e^2\lambda^2}{8\pi^2 c^2 \varepsilon_0 n}\left(\frac{N}{m_e} + \frac{P}{m_h}\right),$$

where e is the elementary charge, λ is the wavelength, c is the speed of light, ε_0 is the vacuum permittivity, n is the intrinsic refractive index, N and P are the electron and hole concentrations, respectively, and m_e and m_h are the effective masses for electrons and holes, respectively.

Bandgap shrinkage occurs due to electron interactions at the conduction band edge and the Pauli exclusion principle, which lead to a lowering of the conduction band minimum (similarly for holes).

In contrast, band filling increases the effective bandgap, as the lower energy states in the conduction band become occupied. As a result, electrons require higher energies for transitions, exceeding the intrinsic bandgap energy E_g.

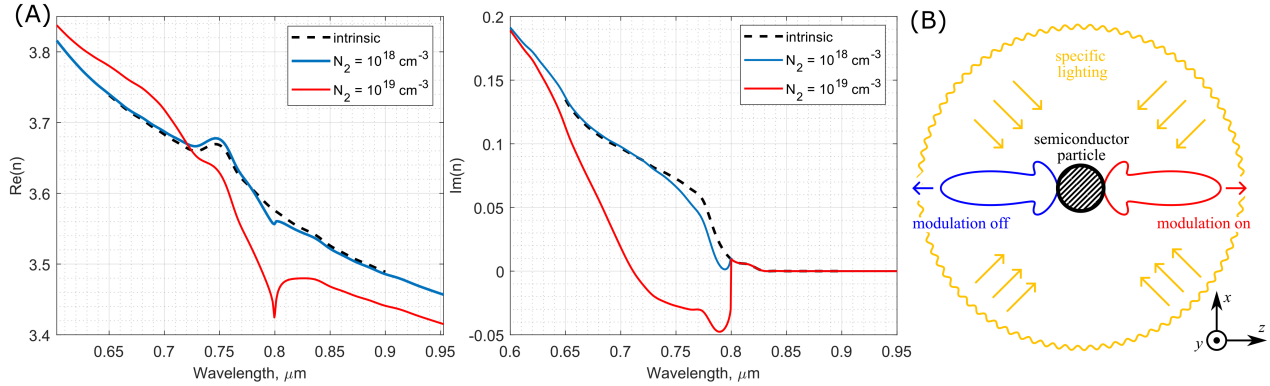

Fig. 1. (A) Refractive index dispersion of $Al_{0.1}Ga_{0.9}As$ for different carrier concentrations: $N_1 = 10^{18}$ cm^{-3} and $N_2 = 10^{19}$ cm^{-3}. (B) Conceptual scheme illustrating scattering direction switching.

These two processes contribute to a change in the optical absorption coefficient, $\Delta\alpha_{\mathrm{BF,\,BS}}(E)$, which is used to calculate the modification of the imaginary part of the refractive index:

$$\mathrm{Im}\Delta n_{\mathrm{BF,\,BS}}(E) = \lambda\Delta\alpha_{\mathrm{BF,\,BS}}(E)/4\pi,$$

while the real part is derived using the Kramers–Kronig relations:

$$\mathrm{Re}\Delta n_{\mathrm{BF,\,BS}}(E) = \frac{ch}{\pi e^2}\int_0^{\infty}\frac{\Delta\alpha_{\mathrm{BF,\,BS}}(E')}{(E'^2 - E^2)}\mathrm{d}E'.$$

Near the bandgap energy, the absorption coefficient for a direct-bandgap semiconductor can be approximated by the following relation:

$$\alpha(E) = C/E\sqrt{E - E_g}\cdot(E > E_g).$$

Its variation due to band filling is calculated using the Fermi–Dirac distribution:

$$\Delta\alpha_{\mathrm{BF}}(E) = \alpha(E)(f(E_v) - f(E_c) - 1),$$

where $f(E) = (1 + \exp[(E_F - E)/k_B T])^{(-1)}$ is the Fermi distribution, and E_v and E_c are the energies of the valence band and conduction band edges, respectively. Bandgap shrinkage reduces the effective bandgap width by ΔE_g [18,22].

Taking both processes into account, the total change in the absorption coefficient is given by [22]

$$\Delta\alpha_{\mathrm{BF,\,BS}}(E) = \alpha(E - \Delta E_g)(f(E_v) - f(E_c)).$$

The contributions from electrons and holes should be calculated separately [18]. The total change in the refractive index is obtained as the sum of the individual contributions:

$$n(N,\,P) = n_0 + \Delta n_{\mathrm{BF,\,BS}} + \Delta n_{\mathrm{FCA}}. \tag{8}$$

Figure 1(A) shows the dispersion dependence of the refractive index and absorption coefficient for different carrier concentrations: $N_1 = 10^{18}$ cm^{-3} and $N_2 = 10^{19}$ cm^{-3} for $Al_{0.1}Ga_{0.9}As$.

C. Light Switching and Excitation of Invisible States

Our goal is to provide an example of a surrounding field in which, at a refractive index n_1, the particle emits radiation in one half-space, and at n_2, it emits in the other half-space. Figure 1(B) schematically shows the geometry of redirecting the field scattered by the particle in different states. According to this setup, for $n = n_1$, the condition $E^s_{1,m} = Q_m E^Q_{1,m}$ should be satisfied, and for $n = n_2$, $E^s_{2,m} = (Q_{-m})^* E^Q_{2,m}$ holds. In this section, we consider the case where $m = 1$ and all other modes are absent. For this reason, we will omit the index m in the notation. Using the relation in Eq. (7), these conditions can be written as

$$E^s_1 = T_1 E^i = Q E^Q_1, \tag{9}$$

$$E^s_2 = T_2 E^i = (Q)^* E^Q_2, \tag{10}$$

where T_1 is scattering matrix of the particle at $n = n_1$, T_2 at $n = n_2$. Thus, if the incident field E^i is a solution, it simultaneously excites non-radiating states in the particle in opposite directions. Similar conditions can be formulated for any azimuthal mode m.

The physical meaning of the derived excitation conditions (9) and (10) can be clarified by drawing an analogy with the well-known Kerker conditions. The Kerker condition $a_{lm} = -b_{lm}$ leads to the suppression of backscattering due to the destructive interference between electric and magnetic dipole contributions. Importantly, this cancellation occurs term-by-term, i.e., within each multipolar order independently.

In contrast, the excitation of Q-modes corresponds to a fundamentally different interference mechanism. Here, the suppression of radiation does not arise from pair-wise cancellation of selected multipoles, but from the coherent superposition of all contributing modes. As a result, the scattering amplitude is minimized through a global interference process involving the full set of multipolar coefficients $\{a_{lm}, b_{lm}\}$. This collective mechanism enables the suppression of radiation not only in a single direction, but over an extended angular range, up to an entire half-space.

Within this framework, the Kerker condition can be interpreted as a limiting case of the more general Q-mode excitation conditions. Specifically, when the multipolar expansion is truncated at $l_{\max} = 1$, the global interference reduces to pair-wise cancellation between the electric and magnetic dipole contributions. For a particular choice of the excitation vector

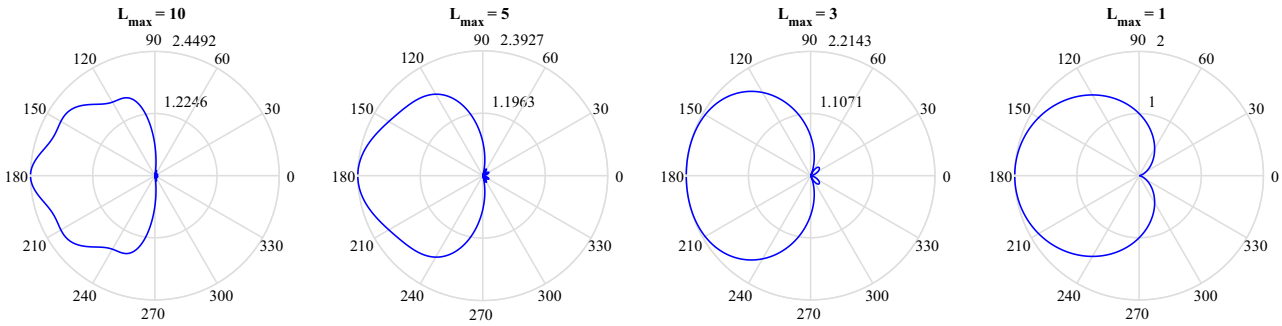

Fig. 2. Connection between the Q-mode excitation condition $E^s = QE^Q$ and the Kerker condition $a_{lm} = -b_{lm}$. The panels show the modulus of the scattering amplitude, $|\mathbf{F}|$, for different values of $l_{\max}$. For the choice of the excitation vector $E^Q \sim (\delta_{lm,11}, -\delta_{lm,11})$ and in the limit $l_{\max} \to 1$, the Q-mode excitation condition exactly reduces to the Kerker condition (rightmost panel).

E^Q, the Q-mode condition continuously transforms into the conventional Kerker condition, as illustrated in Fig. 2.

Nontrivial solutions of Eqs. (9) and (10) do not always exist. For example, if $T_1 = T_2$, these equations reduce to

$$QE_1^Q = (Q)^* E_2^Q,$$

which can only be satisfied if $E_1^Q = E_2^Q = 0$ due to the linear dependence between the even and odd rows of the matrix Q [21]. If the odd rows of QE_1^Q are given by $x_1, x_2, x_3, \ldots$, then the even rows must be uniquely determined by them and are equal to $y_2, y_4, y_6, \ldots$. However, it is evident that for the left-hand side, due to the same linear dependence, these values will be different—$y_2', y_4', y_6', \ldots$—which implies that $QE_1^Q \neq (Q)^* E_2^Q$.

Another extreme case occurs when $T_1 = Q$ and $T_2 = Q^*$; in this situation, due to the relation $Q^2 = Q$ [21], a trivial solution can be obtained by setting $E_1^Q = E_2^Q = E^i$, where E^i can be chosen arbitrarily. The intermediate cases, in which $T_1 \neq T_2$, are more complicated. The question of the existence of a solution and its determination is nontrivial and can be approached in various ways. In every case, one must work with the two columns E_1^Q and E_2^Q, which should be chosen in the most advantageous way from the standpoint of ensuring a solution exists.

A number of approaches have been employed to find solutions in the general case. The most effective method is based on the linear dependence between the even and odd rows of the matrices Q and Q^*. Because of this dependence, it is sufficient to equate only the even (or odd) rows in Eqs. (9) and (10), rather than all rows, while simultaneously choosing the arbitrary columns E_1^Q and E_2^Q such that they are as close as possible to the corresponding vectors $T_1 E^i$ and $T_2 E^i$ in terms of the root-mean-square deviation.

Assume that the scattered field vector E_1^s is known. We choose the product QE_1^Q such that the norm of the difference between these vectors is minimized. This problem is solved by using the pseudoinverse matrix:

$$E_1^Q = Q^\dagger E_1^s,$$

where $Q^\dagger$ is a pseudoinverse of Q. This choice ensures that the difference $|E_1^s - QE_1^Q|$ is minimized. Similarly, one can choose

$$E_2^Q = (Q^*)^\dagger E_2^s.$$

In this case, Eqs. (9) and (10) can be rewritten as

$$QQ^\dagger T_1 E^i = T_1 E^i, \quad Q^*(Q^*)^\dagger T_2 E^i = T_2 E^i.$$

Transferring the left-hand side of the equations to the right-hand side:

$$(QQ^\dagger - I) T_1 E^i = 0, \tag{11}$$

$$(Q^*(Q^*)^\dagger - I) T_2 E^i = 0. \tag{12}$$

The final step involves isolating the even and odd rows. Due to the linear dependence, if $T_1 E^i$ lies within the linear space of Q and the even (or odd) rows are equal to the even (or odd) rows of QE_1^Q, the entire vector $T_1 E^i$ is equal to QE_1^Q. Similarly, the same holds true for $T_2 E^i$ and $Q^* E_2^Q$. Thus, if a solution of the system (11) and (12) exists, the number of equations can be halved by keeping only the even rows in Eq. (11) and the odd rows in Eq. (12). In this case, the system transforms into a square form:

$$(QT)_{1/2} E^i = 0, \tag{13}$$

where the even rows of matrix $(QT)_{1/2}$ are equal to the even rows of matrix $(QQ^\dagger - I)T_1$, and the odd rows of matrix $(QT)_{1/2}$ are equal to the odd rows of matrix $(Q^*(Q^*)^\dagger - I)T_2$. Next, it is necessary to find the nontrivial eigenvectors of matrix $(QT)_{1/2}$ with zero eigenvalues λ:

$$(QT)_{1/2} E_\lambda^i = \lambda E_\lambda^i. \tag{14}$$

The search for eigenvalues was performed numerically, after which values were selected for which the equality holds:

$$\lambda_j^{\text{zero}} = \{|\lambda_i| \lhd 10^{-4},\ i = 1, 2, 3 \ldots\}.$$

If a solution exists, the found eigenvector will be a solution in the sense of the best approximation. For this reason, all found eigenvectors must be verified to satisfy the conditions of Eqs. (9) and (10). The case where no solutions exist will be discussed below.

Since the goal of the work is light switching, in addition to the condition that the scattering amplitudes are equal to zero in the corresponding half-spaces, we aim for the condition that the maximum values of the amplitude functions are equal, to ensure

good contrast in the switching. Furthermore, we seek solutions where the maximum of the incident field is concentrated within the volume of the particle. Otherwise, only a small portion of the incident radiation would interact with the particle. Thus, the desired conditions for a "good" solution are as follows:

1. The scattered field E_1^s does not radiate in the lower half-space ($z < 0$), and the scattered field E_2^s does not radiate in the upper half-space ($z > 0$).
2. The maximum of the scattering amplitude $|\mathbf{F}_1|$ is equal to the maximum of the amplitude $|\mathbf{F}_2|$.
3. The maximum value of the incident field $\mathbf{E}^{\text{inc}}$ is concentrated within the volume of the particle.

Condition 3 is satisfied due to the limited number of modes in the incident field expansion (1). According to the localization principle [23], the term of order l corresponds to a ray passing at a distance of $(l + 1/2)\lambda/2\pi$ from the origin. When $l + 1/2 = 2\pi \mathrm{R}/\lambda = q$, this distance exactly equals the radius of the sphere R, and such terms describe waves that effectively interact with the particle. Terms with $l + 1/2 < q$ correspond to rays falling on the sphere and describe diffraction and scattering processes inside the particle. Thus, we set the number of modes considered in the decomposition of $\mathbf{E}^{\text{inc}}$ in Eq. (1):

$$l_{\max} = \begin{cases} \text{fix}(q) - 5, \text{ if } \text{fix}(q) - \text{odd} \\ \text{fix}(q) - 6, \text{ if } \text{fix}(q) - \text{even} \end{cases},$$

where $\text{fix}(q)$ denotes the nearest integer less than q. We choose different offsets in modes 5 and 6 for even and odd $\text{fix}(q)$ to ensure that $l_{\max}$ is always even, which simplifies the calculations.

Conditions 1 and 2 are not necessarily satisfied during the solution process and therefore require additional verification. To evaluate the efficiency of the switching process, it is useful to introduce a quantitative parameter that characterizes the excitation efficiency of the Q modes:

$$\mathrm{S}^Q = \frac{I^{(\text{forw})} - I^{(\text{back})}}{I}, \tag{15}$$

where $I = \iint |\mathbf{F}| \mathrm{d}\Omega$, $I^{(\text{forw})} = \iint_{\theta \geq \pi/2} |\mathbf{F}| \mathrm{d}\Omega$, $I^{(\text{back})} = \iint_{\theta < \pi/2} |\mathbf{F}| \mathrm{d}\Omega$. The parameter S^Q ranges from -1 to 1. When $\mathrm{S}^Q = -1$, all scattered radiation is directed into the half-space $z < 0$, indicating the excitation of Q-type modes. Conversely, for $\mathrm{S}^Q = +1$, the scattering is directed into the half-space $z > 0$, corresponding to the excitation of Q^*-type modes. To quantify the optical switching between these two states, while taking into account the requirement of equal scattering amplitudes, we define the parameter as follows:

$$\mathrm{S} = \max_{\lambda_j^{\text{zero}}} \left(\frac{1}{2} \frac{S_1^Q \max(|\mathbf{F}_1|) - S_2^Q \max(|\mathbf{F}_2|)}{\max(|\mathbf{F}_1|, |\mathbf{F}_2|)} \right). \tag{16}$$

The quantity S varies from -1 to 1 and characterizes the efficiency of radiation redirection for different refractive indices n_1 and n_2. When $\mathrm{S} = -1$, the particle emits entirely into the half-space $z < 0$ in both states. When $\mathrm{S} = 0$, the radiation is equally distributed in both directions, and no redirection occurs. When $\mathrm{S} = 1$, the radiation in the two states is directed into opposite half-spaces with equal maximum amplitudes. Thus, $\mathrm{S} = 1$ corresponds to the ideal case of optical switching in the chosen metric. In addition, the best solution in Eq. (16), obtained from Eq. (14), is selected among all λ_j^{zero} values.

3. RESULTS

Figure 3 shows the optical switching efficiency S as a function of wavelength and particle radius. The refractive index variation is defined by Eq. (8) and the dependences are shown in Fig. 1(A).

There is a threshold for efficient light-scattering switching around 0.8 μm. This value is determined by the dispersion dependence in Eq. (8), as shown in Fig. 1(A), as noticeable changes in material properties begin after a band gap. Another characteristic feature is the distinct dip around 0.8 μm and the values of R between 4.5 and 6 μm.

A further notable feature is the clear boundary for small sizes ($\mathrm{R} < 1.8$ μm), where no effective light switching occurs. This threshold can be shifted due to different choices of $l_{\max}$. Since the number of modes considered in the particle is insufficient to excite at least one non-radiating state, consequently there are no solutions of Eq. (13). In such cases, we assume $\mathrm{S} = 0$.

The best found value for the S-parameter is $\mathrm{S}_{\max} = 0.8519$ at $\lambda = 0.7206$ μm, $\mathrm{R} = 2.7417$ μm. Figure 4 shows the incident

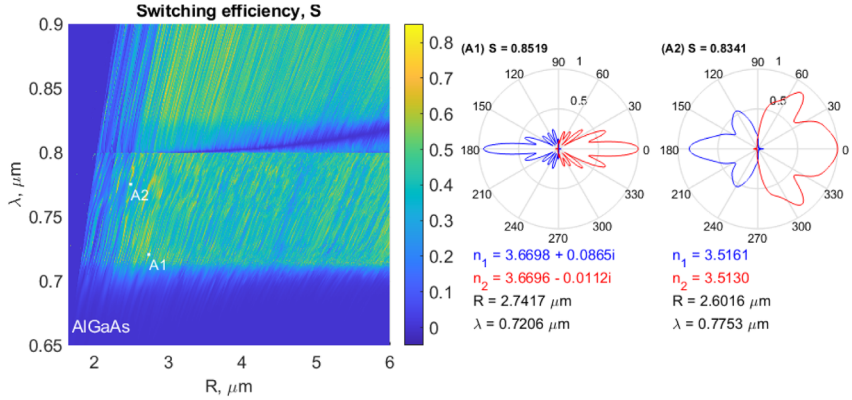

Fig. 3. Optical switching efficiency parameter S as a function of wavelength and particle size. (A) The general distribution of the S-parameter. (A1), (A2)—scattering amplitude moduli for two best S-parameter values: 0.8519, 0.8341, respectively. The blue curves correspond to scattering at $\mathrm{N} = 10^{18}$ cm^{-3}, and the red curves correspond to $\mathrm{N} = 10^{19}$ cm^{-3}. The positions of the points are marked on the graphs with white markers and corresponding labels. The highest value of the S-parameter is achieved at the point A1.

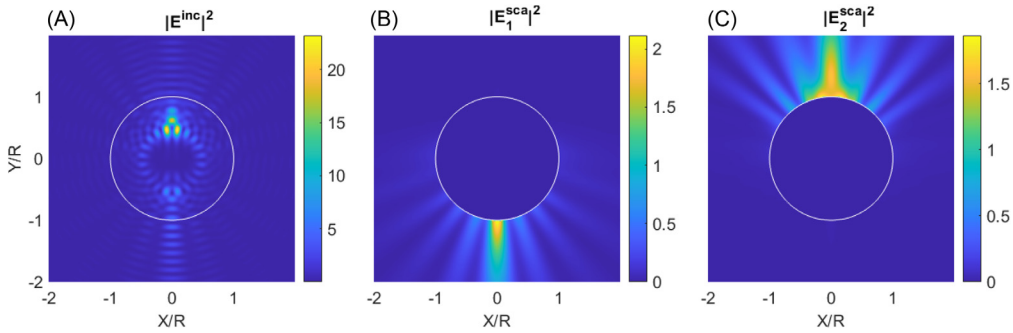

Fig. 4. (A) Incident radiation on the particle. (B) Scattered field at $N = 10^{18}$ cm^{-3}. (C) Scattered field at $N = 10^{19}$ cm^{-3}, for AlGaAs. Radiation and particle parameters: $\lambda = 0.7206$ μm, $R = 2.7417$ μm, and $S = S_{max} = 0.8519$ [point A1 in Fig. 3(A)]. Note that the maximum value of $|\mathbf{E}^{inc}|^2$ outside the particle is approximately 4.5. Therefore, the fields $|\mathbf{E}_1^{sca}|^2$, $|\mathbf{E}_2^{sca}|^2$ are comparable in magnitude to $|\mathbf{E}^{inc}|^2$.

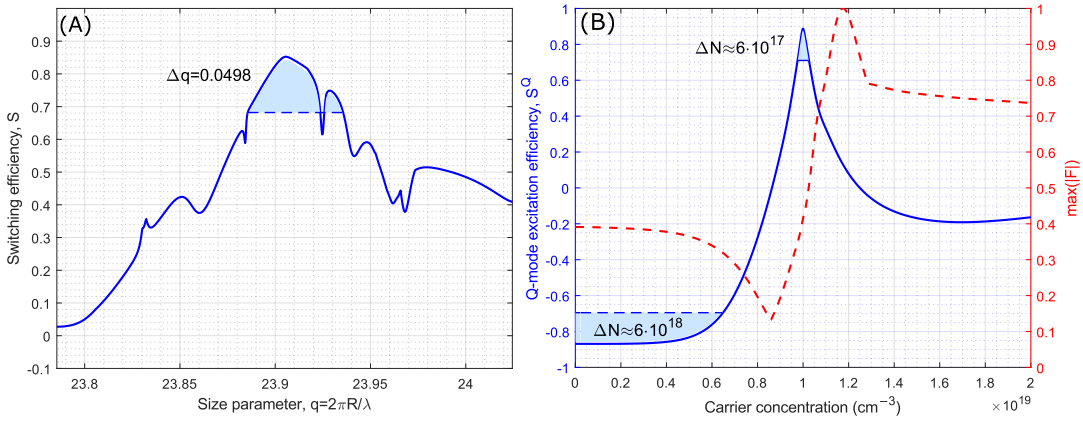

Fig. 5. (A) Optical switching efficiency S versus the size parameter $q = 2\pi R/\lambda$ for a particle in a fixed external field $\mathbf{E}^{inc}$. (B) Q-mode excitation parameter S^Q as a function of carrier concentration N. The red dashed curve indicates the normalized scattering amplitude maximum $|\mathbf{F}|$. Results are shown near the resonance point A1 in Fig. 3.

and scattered fields of the particle at different refractive indices, corresponding to the point of maximum switching efficiency.

4. DISCUSSION

Figure 3 exhibits pronounced oscillations, since at each point a new external field configuration is selected. To accurately estimate the actual resonance width, the external field must be fixed. As an example, let us consider the accuracy of the system parameters at the point of maximum switching, labeled A1. Figure 5(A) shows the switching efficiency as a function of the size parameter $q = 2\pi R/\lambda$ calculated for a fixed incident field $\mathbf{E}^{inc}$.

The width of the considered resonance, determined as the range where the parameter S deviates by no more than 80% from its maximum value, is estimated to be $\Delta q = 2\pi\,\Delta(R/\lambda) \approx 0.05$. This corresponds to a wavelength variation of approximately $\Delta\lambda \sim 1.5$ nm for a fixed particle radius R, which is readily achievable with a wide class of laser sources. Note that the transition width $\Delta\lambda$ depends on the region in which it occurs; for instance, for point A2 in Fig. 3, it is an order of magnitude larger, reaching $\Delta\lambda = 15$ nm, while the dependence in Fig. 5(A) shows a smooth curve with a single maximum.

Let us now consider the dynamics of the radiation pattern evolution when the carrier density N deviates from its limiting values N_1 and N_2. When pumping the material with ultrashort laser pulses, this transition can occur on time scales of the order of 10^{-13} s. The incident field, particle size, and wavelength are assumed to be fixed. The parameter S characterizes the optical switching between two states; however, to analyze the dynamics of the radiation pattern evolution, it is convenient to introduce the parameter S^Q. Figure 5(B) shows the dependence of S^Q on the carrier density N. The ideal switching scenario corresponds to the points where S^Q changes from -1 to 1 under the condition of equal maximum field amplitudes $\mathbf{F}$. In this case, the overall switching efficiency parameter S reaches unity. In the considered example, the best value of $S = 0.85$ is obtained for carrier densities of $N_1 = 10^{18}$ cm^{-3} and $N_2 = 10^{19}$ cm^{-3}. As can be seen from the graph, this value remains nearly constant over relatively broad ranges of N_1 and N_2.

In the present analysis, the refractive index of the particle is assumed to vary uniformly. If the refractive index changes nonuniformly, the above considerations remain valid; however, the scattering matrices T_1 and T_2 in Eqs. (9) and (10) have different elements. The existence of such solutions in the nonuniform case requires a separate analysis, but no fundamental limitations arise in this respect.

To implement the proposed concept of light-scattering control, two additional tasks must be addressed: (i) generating the required carrier density N within the particle and (ii) constructing a resonant structure or optical system that supports the necessary spatial modes. Both tasks are nontrivial but can be realized using several approaches.

The charge carrier density can be altered by electrical or optical pumping. To realize the required spatial field distribution, an optical system comprising at least two lenses placed on opposite sides of the particle is required, since the incident field $\mathbf{E}^{\mathrm{inc}}$ is generally non-unidirectional. These lenses can be positioned in the far field, as the desired field contains no evanescent spatial harmonics due to its representation as a series of spherical functions of the first kind. The simplest technique for generating the required fields is to project the Fourier spectrum of the desired radiation onto the lens aperture, whereby the lens forms its Fourier transform in the focal plane, producing the necessary field distribution.

Finally, we note that the estimates presented above are primarily of a qualitative nature. The exact resonance widths may vary depending on the particle geometry and illumination wavelength. The main goal of this section is to demonstrate the principal feasibility of the described effect. Moreover, in a practical implementation, some of the constraints introduced in this study can be relaxed.

5. CONCLUSION

We have theoretically demonstrated the possibility of light switching based on the excitation of half-space invisible states in semiconductor microparticles. Using the developed matrix formalism, we analyzed the field distributions corresponding to non-radiating configurations localized within a given half-space. The conditions for optical switching of radiation scattering between two half-spaces due to the excitation of non-radiating modes are presented. It is shown that the solution retains its essential properties under small variations of the system parameters. These results deepen the physical understanding of light–matter interaction in mesoscale systems and open new perspectives for the design of tailored scattering responses.

Funding. Foundation for the Advancement of Theoretical Physics and Mathematics (501100012708) (23-1-1-61).

Disclosures. The authors declare no conflicts of interest.

Data availability. Data are available upon reasonable request.

REFERENCES

1. A. I. Kuznetsov, A. E. Miroshnichenko, M. L. Brongersma, *et al.*, "Optically resonant dielectric nanostructures," Science **354**, aag2472 (2016).
2. C. W. Hsu, B. Zhen, J. Lee, *et al.*, "Observation of trapped states in the continuum," Nature **499**, 188–191 (2013).
3. K. Koshelev, G. Favraud, A. Bogdanov, *et al.*, "Non-Hermitian photonics based on bound states in the continuum," Nanophotonics **8**, 725–745 (2019).
4. Z. Wang, W. Guo, L. Li, *et al.*, "Optical virtual imaging at 50 nm resolution through a blue-ray DVD disk and a micro-sphere lens," Nat. Commun. **2**, 218 (2011).
5. D. G. Baranov, S. V. Makarov, A. E. Krasnok, *et al.*, "Tuning of near- and far-field properties of all-dielectric dimer nanoantennas via ultrafast electron-hole plasma photoexcitation," Laser Photonics Rev. **10**, 1009–1015 (2016).
6. W. Liu and Y. S. Kivshar, "Generalized Kerker effects in nanophotonics and meta-optics," Opt. Express **26**, 13085–13105 (2018).
7. A. Heifetz, J. J. Simpson, S. C. Kong, *et al.*, "Subdiffraction optical resolution of a gold nanosphere located within the nanojet of a Mie-resonant dielectric microsphere," Opt. Express **15**, 17334–17342 (2007).
8. Z. Wang, B. Luk'yanchuk, L. Yue, *et al.*, "High-order Fano resonances and giant magnetic fields in dielectric microspheres," Sci. Rep. **9**, 20293 (2019).
9. A. Darafsheh, "Photonic nanojets and their applications," J. Phys. Photonics **3**, 022001 (2021).
10. N. Yu and F. Capasso, "Flat optics with designer metasurfaces," Nat. Mater. **13**, 139–150 (2014).
11. M. Decker, I. Staude, M. Falkner, *et al.*, "High-efficiency dielectric Huygens' surfaces," Adv. Opt. Mater. **3**, 813–820 (2015).
12. A. R. Bekirov, B. S. Luk'yanchuk, E. I. Elyas, *et al.*, "Half-space invisible states in dielectric particles," Opt. Express **31**, 37074–37081 (2023).
13. T. Badloe, J. Lee, J. Seong, *et al.*, "Tunable metasurfaces: the path to fully active nanophotonics," Adv. Photonics Res. **2**, 2000205 (2021).
14. D. G. Baranov, D. A. Zuev, S. I. Lepeshov, *et al.*, "All-dielectric nanophotonics: the quest for better materials and fabrication techniques," Optica **4**, 814–825 (2017).
15. M. R. Shcherbakov, P. P. Vabishchevich, A. S. Shorokhov, *et al.*, "Ultrafast all-optical switching with magnetic resonances in nonlinear dielectric nanostructures," Nano Lett. **15**, 6985–6990 (2015).
16. M. R. Shcherbakov, S. Liu, V. V. Zubyuk, *et al.*, "Ultrafast all-optical tuning of direct-gap semiconductor metasurfaces," Nat. Commun. **8**, 17 (2017).
17. M. A. Butt, "Emerging trends in thermo-optic and electro-optic materials for tunable photonic devices," Materials **18**, 2782 (2025).
18. B. R. Bennett, R. A. Soref, and J. A. D. Alamo, "Carrier-induced change in refractive index of InP, GaAs and InGaAsP," IEEE J. Quantum Electron. **26**, 113–122 (1990).
19. P. C. Waterman, "Matrix formulation of electromagnetic scattering," Proc. IEEE **53**, 805–812 (1965).
20. S. Stein, "Addition theorems for spherical wave functions," Q. Appl. Math. **19**, 15–24 (1961).
21. A. Bekirov, "On superresolution in virtual image in a transparent dielectric sphere," Opt. Spectrosc. **131**, 037001 (2023).
22. L. Shen, P. J. Van Veldhoven, Y. Jiao, *et al.*, "Ohmic contacts with ultra-low optical loss on heavily doped n-type InGaAs and InGaAsP for InP-based photonic membranes," IEEE Photonics J. **8**, 4500210 (2016).
23. H. C. van de Hulst, *Light Scattering by Small Particles* (Courier Corporation, 1981).